ORIGINAL PAPER

Improvement of mechanical, morphological and thermal properties on PP-enriched graphene oxide/PP-g-MA/EPDM blend compatibilized: PP-g-MA compatibilizer and graphene oxide nanofiller role

Mohammad Javad Azizli[1] · Mohammad Barghamadi[2] · Katayoon Rezaeeparto[3] · Somayeh Parham[3]

Abstract

One of the modern methods of mixing polymers that causes the properties of nanocomposites to be significantly improved is the incorporation of nanofillers into the matrix. In this study, polypropylene (PP) was reinforced using graphene oxide and then PP-g-MA compatibilizer was used for better dispersion of graphene oxide and compatibility between polypropylene and ethylene-propylene rubber (EPDM). The purpose of this study is to achieve the optimum blend composition. In this regard, the mechanical, rheological and morphological properties of samples using DMTA, TGA and DSC were examined and their theory was analyzed. The results showed that the mechanical properties such as tensile strength, elongation at break and young's modulus are significantly improved by increasing the concentration of graphene oxide in the presence of PP-g-MA compatibilizer. SEM images also illustrated that with the increasing concentration of nanofillers in the blend matrix, the particle size of the dispersed phase of EPDM decreases. In addition, TEM images also showed the presence of PP-g-MA compatibilizer causing better dispersion of graphene oxide in GO-PP/ PP-g-MA/EPDM nanocomposites.

Keywords Graphene oxide · GO-PP/PP-g-MA/EPDM · Mechanical properties · Christensen-Lo theory · Creep behaviour

Introduction

PP is a common semi-crystalline thermoplastic that has been widely used in various applications. This is due to the versatile properties, low price with easy processing of this thermoplastic. PP is a free-color material and has high chemical resistance and high-temperature resistance [1]. Experiments demonstrated that it has suitable physical and mechanical properties at room temperature. PP is comparatively stiff and has a great melting point, low density and impact resistance [2]. The blending of various polymers has been extensively used to tailor materials in particular applications with low prices in comparison with developing a novel polymer [3]. PP is frequently manufactured in the form of a PP/EPDM blend. They are specified with a raised resistance to impact in a broad temperature range [4]. However, its application is confined when the thermo-mechanical characteristics merged with excellent rigidity and resistance to temperature are needed [5]. To achieve this goal, the combination of these two polymers and the use of their advantages along with the creation of nanocomposites containing nanoparticles with desirable properties, are considered [6]. However, the major challenge in the preparation of these nanocomposites is the dispersion of nanoparticles within blends. Therefore, the addition of compatibilizers is often needed to attain the well-dispersed morphology for better properties [7].

Recently, graphene oxide (GO) has transpired as a novel carbon material with nano size and excellent mechanical characteristics [8]. The GO prepared by chemical exfoliation of graphite has functional groups such as hydroxyls, epoxides, diols, ketones and carboxyls. However, the chemical functionality extensively changes the interactions between the nanosheet agglomerates and then is easily dispersed in the matrix [9].

✉ Mohammad Javad Azizli
MohammadJavad.azizli@gmail.com;
MohammadJavad.azizli@yahoo.com

1   Department of Chemistry and Chemical Engineering, Islamic Azad University, Rasht BranchRasht, Iran

2   Iran Polymer and Petrochemical Institute, P. O. Box, Tehran 14965-115, Iran

3   Research Institute of Petroleum Industry, P. O. Box, Tehran 14857-33111, Iran

Haghnegahdar et al. [10] prepared the PP/EPDM/graphene nanocomposites by the melt mixing process. The effect of graphene on the microstructure and fracture toughness was investigated. They reported that the graphene nanoplatelets acted as obstacles against crack propagation. In the study by Doufnoune et al. [7] PP/EPDM with different amounts of partially reduced graphene oxide (prGO) were investigated. Mechanical tests showed that the incorporation of prGO to the PP/EPDM blend enhanced the tensile strength and Young's modulus while decreasing the elongation at break. TGA analysis illustrated that the nanocomposites exhibited higher thermal stability than that of the neat matrix. In another work, Diez-Pascual [11] investigated the effect of GO on the mechanical, thermal, and morphological properties of nanocomposites based on PP/EPDM. The addition of GO improved the tensile strength and Young's modulus of PP/EPDM nanocomposite. While the elongation and Izod impact strength were adversely affected. Furthermore, the TGA analysis showed that the incorporation of GO improves significantly the thermal stability of nanocomposites.

The major purpose of this paper is to investigate the effect of graphene oxide nanoparticles and compatibilizers on the characteristics of PP/EPDM-based nanocomposites produced with the melt mixing method. The effect of graphene oxide nanoparticles incorporation and usage of PP-g-MA compatibilizer on the morphology, thermal, mechanical and rheological properties of the nanocomposites were examined.

Experimental

Materials

PP with specification: Vicat softening point (9.8 N): 135 ± 2 °C, Density 0.91 g/cm^3 and also H.D.T. (0.5 Mpa): 80 ± 2 °C. EPDM with specification: Mooney viscosity ML (1 + 4) at 100° C of 68 ± 2, the density of 0.82 g/cm^3, ethylene content of 67% and ENB of 4.3%. The maleic

anhydride-modified polypropylene (PP-g-MA) Epolene G3015 (MA = 1.3%, MW = 47,000 g mol, and also acid number = 15 mg of KOH/g PPMA,) was obtained from Eastman Chemical company. The graphene oxide (GO) with specification: surface area of about 740 m^{2}g^{-1} and also thickness of 5–10 nm. Table 1 lists the names of the materials used, the amount of each of them and the source of their preparation. In all of the samples, P, E, M and G are the acronym for the PP, EPDM, PP-g-MA and GO, respectively. For example, P80/E20/M5/G1 represents a sample containing 80 phr of PP, 20 phr of EPDM, 5 phr of PP-g-MA and 1 phr of GO.

Sample Preparation

To enhance the dispersion of GO in the matrix, the mixture of HCOOH and DMF was used [12]. For this purpose, 5 g of PP in 50 mL of HCOOH at 58 °C was stirred. Then, nanoparticles were distributed in 200 mL of the DMF/HCOOH mixture (4:1). This mixture was sonicated in 50 min and poured in PP/HCOOH. The DMF alters the phase separation because this material is non-solvent for PP [13]. PP/GO was rinsed off in a coagulation bath [14]. The nanocomposites were filtered in a vacuum oven and homogenized. Then, it was rinsed with water to reach neutral pH and finally dried at 120 °C for 11 h. The floated mixture was diluted with fresh PP to attain the final concentration of nanoparticles at the solid state. After that, the samples were compressed and molded in a Carver laboratory press at 180 °C and a pressure of 140 bar. The schematic representation of the nanocomposite preparation is illustrated inFig. 1.

The different formulations of blends were prepared by melt mixing method in a Brabender (W50, Germany) for 5 min at 80 rpm and 110 °C. After that, The EPDM was added to the mixture and the preparation is continued for 4 min. In the next step, activators such as zinc oxide and stearic acid were incorporated, and mixing continued for 4 min. At last, the accelerators such MBTS and TMTD and also curing agent containing Sulphur mixed for 3 min.

Table 1 Formulation of GO-PP/PP-g-MA/EPDM blends

Ingredient	Role	Content (phr)	Supplier	Trade name
PP	Matrix phase	80	Marun (Iran)	MOPLEN-MR230C
EPDM	Disperse phase Compatibilizer	20	LANXESS (Germany)	Keltan, 778 Z
PP-g-MA	Activator	5	Uniroyal (USA)	Royaltuf 465A
Stearic acid	Activator	1.5	AG (Germany)	-
Zinc oxide	Curing agent	5	AG (Germany)	-
Sulfur	Accelerator	1	AG (Germany)	-
TMTD a	Accelerator	1	LANXESS (Germany)	-
MBTS b	Nanofiller	1	LANXESS (Germany)	-
Graphene Oxide		1, 3, 5,7 and 1	XG Sciences (USA)	C 750

a. Tetra-methyl thiuram disulfide

b. Mercapto benzothiazole disulfide

Table 2 The average number radius, average volume radius and polydispersity index for GO-PP/PP-g-MA/EPDM nanocomposites

PDI	R_v(μm)	R_n(μm)	Sample
5.86	42.36	11.44	P80/E20
4.81	37.18	9.98	P80/E20/M5
3.21	12.44	7.73	P80/E20/M5/G 0.1
2.92	8.85	6.04	P80/E20/M5/G 0.3
2.81	6.57	4.92	P80/E20/M5/G 0.5
2.47	5.96	3.79	P80/E20/M5/G 0.7
2.28	5.9309	3.14	P80/E20/M5/G 1

Characterization

Morphological analysis

Field emission scanning electron microscopy (SEM) Vega II Tescan model made in the Czech Republic was used to study the microstructure of nanocomposites. To prepare the samples, the nanocomposites were broken in liquid nitrogen. Transmission electron microscopy (TEM) tests were applied by LIBRA 200MC model made in Germany with a 120 kV operating voltage. Thin layers of nanocomposites with a thickness of about 70 nm were cut with an ultramicrotome EM UC/FC6 made in Austria at a temperature of -120 °C.

Thermal Properties

The Differential Scanning Calorimetry (DSC) of nanocomposites was examined using Labsys TG made by SETARAM Instrumentation. All the measurements were performed in the nitrogen atmosphere. At all stages, the temperature change rate was constant at 10 °C/min. Equation (1) was used to measure the crystallinity:

$$X = \frac{\Delta H_m}{\Delta H_{max} \times m} \times 100 \tag{1}$$

where ΔH_m is the melting enthalpy, ΔH_{max} is the enthalpy of 100% PP crystalline and m is the weight percentage of PP in the nanocomposites.

The Thermal Gravimetric Analysis (TGA) of nanocomposites was applied using Labsys TG made by SETARAM Instrumentation in a nitrogen atmosphere at a temperature range of 0 to 600 °C, and a constant heating rate of 10 °C/min.

Mechanical Testing

Tensile testing of samples was performed using model AI-7000-SU1 made in Germany by ASTM D 638 standard at a tension rate of 50 mm/min at room temperature. To measure the hardness of samples (Shore D), the Zwick machine 3100 made in Germany following ASTM D 2240 standard was used. Zwick's HIT model 5113–5.5 J made in Germany according to ASTM D 256 standard was also used to measure the impact strength of the nanocomposites.

Dynamic Mechanical Thermal Analysis (DMTA)

Dynamic mechanical thermal analysis (DMTA) was performed to evaluate the compatibility of the nanocomposites using the Triton Tritic 2000 device. This test was applied at a frequency of 1 Hz with a temperature range of -100 °C to 100 °C and a heating rate of 5 °C/min.

Rheological Testing

The rheological behavior and linear viscosity properties of the melt samples were measured with a Zwick dynamic rheometer model 4308 manufactured by Zwick company at a temperature of 100 °C. A frequency sweep test was performed from 0.04 rad/s to 600 rad/s. A strain level of 1% was used in all tests to investigate the material response in the linear viscosity region.

Table 3 Non-isothermal crystallization and melting parameters of the GO-PP/PP-g-MA/EPDM nanocomposites

X_c (%)	Melting Enthalpy ΔH_m (J/g)	Peak Melting Temp (°C)	Crystallization Enthalpy ΔH_c (J/g)	Peak Temp T_{cp} (°C)	Initial Crystallization Temp T_c (°C)	Samples
22.11	53.11	168.2	48.11	146.8	151.3	**P80/E20**
22.19	54.04	169.7	49.08	147.9	152.5	**P80/E20/M5**
23.87	55.88	171.6	51.02	150.1	155.9	**P80/E20/M5/G 0.1**
25.01	56.01	173.4	52.88	152.8	158.3	**P80/E20/M5/G 0.3**
26.03	57.18	175.3	54.03	155.1	160.8	**P80/E20/M5/G 0.5**
27.44	57.33	177.8	54.76	158.2	162.9	**P80/E20/M5/G 0.7**
28.36	57.53	179.7	54.98	161.1	164.7	**P80/E20/M5/G 1**

Table 4 Thermal properties of P80/E20 based nanocomposites

Blends	T_2 [A] (ºC)	T_{10} [B] (ºC)	T_{50} [C] (ºC)	ML at 300 ºC [D] (wt.%)	ML at 500 ºC [E] (wt.%)	Char residue at 600 ºC (wt.%)
P80/E20	288.35	388.22	450.16	4.77	90.87	8.27
P80/E20/M5	288.57	388.41	450.28	4.71	90.74	8.31
P80/E20/M5/G 0.1	289.42	389.89	452.57	4.45	88.24	9.87
P80/E20/M5/G 0.3	290.08	391.42	454.63	3.98	86.41	10.05
P80/E20/M5/G 0.5	291.44	392.96	456.62	3.74	84.36	11.77
P80/E20/M5/G 0.7	292.38	393.47	458.23	3.73	82.54	13.09
P80/E20/M5/G 1	293.87	395.49	460.23	3.11	81.25	15.42

[A–C] Decomposition temperature at 2, 10 and 50% mass loss, respectively, and

[D–E] mass loss at 300, 500 and 600 ºC temperature

Results and Discussion

Morphological observations

Figure 2 compares the SEM image of the GO-PP/PP-g-MA/EPDM compatibilized nanocomposites. Figure 2a shows a neat sample of PP/EPDM and Fig. 2b compares a sample of PP/PP-g-MA/EPDM and shows the effect of the PP-g-MA compatibilizer. It is well known that the addition of PP-g-MA reduces the average size of EPDM dispersed phase droplets. This is probably due to the compatibility between these two incompatible polymers. Figures 3c-g also compare the effect of increasing graphene oxide in the presence of PP-g-MA compatibilizer. As the concentration of graphene oxide increases, in addition to the improvement in distribution and dispersion, the average size of EPDM dispersed phase droplets decreases. This possibility is due to the good interaction of EPDM and PP polymers with PP-g-MA and graphene oxide compatibility (cf. Fig. 3).

Equations 2 to 4 were applied for the analysis to obtain the average number of droplet radius ($\overline{R}_n$), the average volume radius ($\overline{R}_v$) and the polydispersity index (PDI) of the droplet phase in the blend matrix [15]:

$$\overline{R}_n = \frac{\sum n_i R_i}{n_i} \tag{2}$$

$$\overline{R}_v = \frac{\sum n_i R_i^4}{\sum n_i R_i^3} \tag{3}$$

$$PDI = \frac{\overline{R}_v}{\overline{R}_n} \tag{4}$$

In the above equations, n_i and R_i are droplet number and droplet radius. Table 2 illustrates the values of $\overline{R}_n$, $\overline{R}_v$ and PDI for nanocomposites reinforced by various levels of graphene oxide with and without PP-g-MA compatibilizer. From the table results, it can be shown that the P80/E20/M5/G1 nanocomposite shows the lowest droplet radius for the EPDM phase. Graphene oxide nanoparticles change the viscosity ratio of PP/EPDM blend, hence, altering the droplet break-up rate [16]. Further, graphene oxide nanoparticles in the PP/EPDM matrix maybe play a role as a barrier to the reduction of dispersed phase matrix [17]. Scaffaro et al. [18], represented that nanoparticles extremely reduce the dispersed size of droplets as compatibilizer effect and destruction of droplet coalescence.

Table 5 Mechanical properties of GO-PP/PP-g-MA/EPDM nanocomposites

Hardness (Shore D)	Elongation at Break (%)	Young Modulus (MPa)	Impact Strength (kJ/m²)	Tensile Strength (MPa)	Blends
58.3 ± 1.1	391 ± 8	226.3 ± 4	26.7 ± 0.52	17.4 ± 0.34	**P80/E20**
58.8 ± 1.1	398 ± 8	229.8 ± 5	26.9 ± 0.56	17.9 ± 035	**P80/E20/M5**
61.2 ± 1.2	408 ± 8	331.6 ± 6	28.3 ± 0.59	20.1 ± 0.41	**P80/E20/M5/G 0.1**
65.4 ± 1.3	411 ± 8	348.5 ± 7	30.2 ± 0.65	23.4 ± 0.47	**P80/E20/M5/G 0.3**
68.9 ± 1.4	416 ± 8	359.7 ± 7	32.3 ± 0.62	26.8 ± 0.53	**P80/E20/M5/G 0.5**
71.8 ± 1.4	425 ± 8	374.3 ± 8	34.6 ± 0.68	29.4 ± 0.59	**P80/E20/M5/G 0.7**
72.6 ± 1.4	424 ± 9	379.1 ± 8	35.9 ± 0.71	30.1 ± 0.61	**P80/E20/M5/G 1**

Table 6 Loss factor and storage modulus results for GO-PP/PP-g-MA/EPDM nanocomposites

Blends	Tg from E′ [ºC]	Tg from tan δ [ºC]	Height of Tg peak [-]	Decrease in tan δ peak [-]	E' at 25ºC [MPa]
P80/E20	-8.89	-10.06	5.96	0	2.88
	-51.79	-54.01	1.38	0	4.06
P80/E20/M5	-8.05	-9.83	5.32	0.64	4.33
P80/E20/M5/G 0.1	-6.33	-8.02	4.42	1.54	5.56
P80/E20/M5/G 0.3	-4.84	-6.59	3.89	2.07	6.09
P80/E20/M5/G 0.5	-3.16	-5.06	3.31	2.65	6.71
P80/E20/M5/G 0.7	-1.87	-3.94	2.71	3.25	7.66
P80/E20/M5/G 1	-1.03	-2.47	2.18	3.78	8.06

Figure 4 compares the TEM images of GO-PP/PP-g-MA/EPDM nanocomposites to observe the compatiblizing effect of PP-g-MA on the distribution and dispersion of graphene oxide. In the non-compatibilized sample i.e. P80/E20/G1, graphene oxide has aggregated in the PP phase due to the higher polarity than the EPDM phase which is also mentioned in the work of McKeen [19]. So, two separate phases are illustrated. However, in the P80/E20/M5/G1 sample, the nanocomposite containing PP-g-MA compatibilizer, a proper dispersion of graphene oxide in the GO-PP/PP-g-MA/EPDM blend matrix. Therefore, a uniform state of dispersed graphene oxide within the matrix is achieved [20].

Differential scanning calorimetry (DSC) measurements

A study of the effect of graphene oxide and PP-g-MA compatibilizer on the melting and non-isothermal crystallinity properties of GO-PP/PP-g-MA/EPDM nanocomposites was performed using a DSC device. The DSC results are shown in Fig. 5 and the main parameters included in Table 3. PP is a semi-crystalline polymer with a relatively high crystalline range and a high crystallization temperature, while EPDM is an amorphous polymer. As the DSC thermograms (Fig. 5a) show, for the neat PP/EPDM blend a crystallization peak is observed upon cooling, which the amount of this peak increases by the addition of PP-g-MA compatibilizer and the incorporation of 0.1 phr of graphene oxide to the neat blend. The main reason for this phenomenon is the acceleration of nucleation and crystallization by graphene oxide nanosheets with the help of PP-g-MA compatibilizer. The presence of graphene oxide nanoparticles with PP-g-MA compatibilizer leads to more efficient nucleation and increases the crystallization temperature in the polypropylene matrix [21]. Figure 5b illustrates the thermograms of the reheating step of the nanocomposites. By calculating the crystallization percentage from the melting curve in this step, it is determined that by adding PP-g-MA compatibilizer and 0.1 phr of graphene oxide, the crystallization percentage increases due to the nucleation effect of graphene nanoparticles. Also, with increasing graphene oxide concentration, the amount of crystallization temperature increases and the crystallization percentage is raised. Because, the placement of PP/PP-g-MA/EPDM blend chains in the vicinity of graphene oxide plates and interaction with the nanoparticles, causes the chains to move in the crystal lamella. This is due to the widespread dispersion of graphene oxide with the help of PP-g-MA compatibilizer. Another point in these results is the increase in ΔH_m and ΔH_c in the GO-PP/PP-g-MA/EPDM nanocomposites with increasing the graphene oxide concentration, compared to the neat PP/EPDM blend, which indicates the role of graphene oxide in increasing the crystallization rate of PP [22].

Thermal stability

The results of the weight loss profile of the neat and nanocomposites based on PP/EPEM blend with and without compatibilizer are shown in Fig. 6 and the main parameters are included in Table 4. As it can be seen, the thermal degradation resistance of PP/PP-g-MA/EPDM nanocomposites increases with increasing graphene oxide levels. So that the required temperature for the thermal degradation of the sample is significantly increased by increasing the 1 phr of graphene oxide in the presence of the PP-g-MA compatibilizer. The reason for this is the graphene oxide nanosheets that act as a barrier against the penetration of oxygen inside the structure and delay the thermal degradation and thus improve the thermal stability. Furthermore, the neat PP/EPEM blend has a wide degradation peak and by adding graphene oxide nanoparticles in the presence of PP-g-MA compatibilizer, the degradation peak becomes sharper and

Table 7 Herschel-Bulkley model parameters for GO-PP/PP-g-MA/EPDM nanocomposites

| n	K	$\sigma_0 = G_0^* \dot{\gamma}$ (Pa)	Blends
0.79	1203.1	2.39	P80/E20
0.79	1288.9	3.01	P80/E20/M5
0.76	1441.3	18.41	P80/E20/M5/G 0.1
0.74	1589.6	26.38	P80/E20/M5/G 0.3
0.71	1987.8	56.23	P80/E20/M5/G 0.5
0.68	2274.4	63.54	P80/E20/M5/G 0.7
0.66	2667.8	69.15	P80/E20/M5/G 1

**Fig. 1** The Schematic representation of the PP/GO preparation
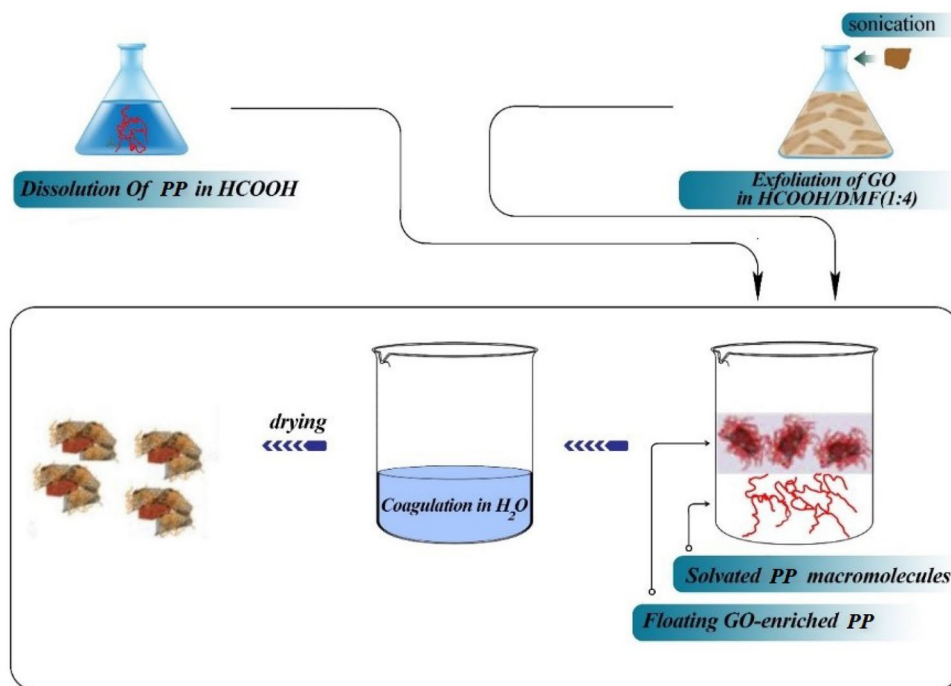
transferred to higher temperatures. In Table 4, the decomposition temperature at 2, 10 and 50% mass loss and mass loss (ML) at 300, 500 and 600 ℃ temperatures for the nanocomposites are shown. As can be seen, the decomposition temperature of nanocomposites in three different weight loss is raised which shows the enhanced thermal stability of the incorporation of nanosheets. In other words, graphene oxide nanosheets stabilize phase morphology and improve the interfacial interaction of the GO-PP/PP-g-MA/EPDM polymer blend. These observations confirm the results of rheological and morphological studies and also DMTA tests. Also, the weight percentage of residual material of nanocomposites at three various temperatures i.e. 300, 500 and 600 ℃ compared to the neat blend illustrated that by increasing the graphene oxide concentration in the presence of PP-g-MA compatibilizer, the residual minerals increase [23].

The mechanical characteristics of nanocomposites based on PP/EPDM with and without compatibilizer reinforced by various levels of graphene oxide are tabulated in Table 5. As it can be seen, adding the PP-g-MA compatibilizer and GO nanoplatelets serves to improve the mechanical properties of GO-PP/PP-g-MA/EPDM nanocomposites. It is reported in the kinds of literature that the addition of nano-reinforcements to the polymers raises the impact strength, tensile properties, hardness and modulus, and on the other hand declines the elongation. This attributes the intrinsic nature and also the rigidity of the graphene oxide nanosheets [24]. According to Table 5, in the presence of the PP-g-MA compatibilizer, the impact strength, tensile properties and rigidity significantly raised is attributed to the very well interaction of GO and

polymeric chains in the GO-PP/PP-g-MA/EPDM nanocomposites (cf. to Fig. 2). Given that the surface area of graphene oxide is high, the incorporation of these nanoparticles throw polymer chains in the presence of compatibilizer, serves to enhance the mechanical performance of the GO-PP/PP-g-MA/EPDM nanocomposites. In another word, the filler–polymer interactions in the interphase caused reduction of mobility in the molecular scale in the sample structure [25]. The raising of hardness by increasing the graphene oxide levels of the GO-PP/PP-g-MA/EPDM nanocomposites is usually attributed to the rigid nature of carbonaceous reinforcements [26]. The mechanical characteristics also illustrate enhanced to 0.7 phr
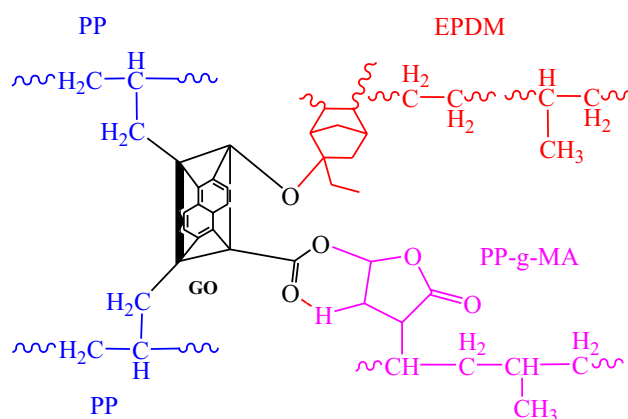
Fig. 2 The chemical interactions between GO, PP, PP-g-MA and EPDM
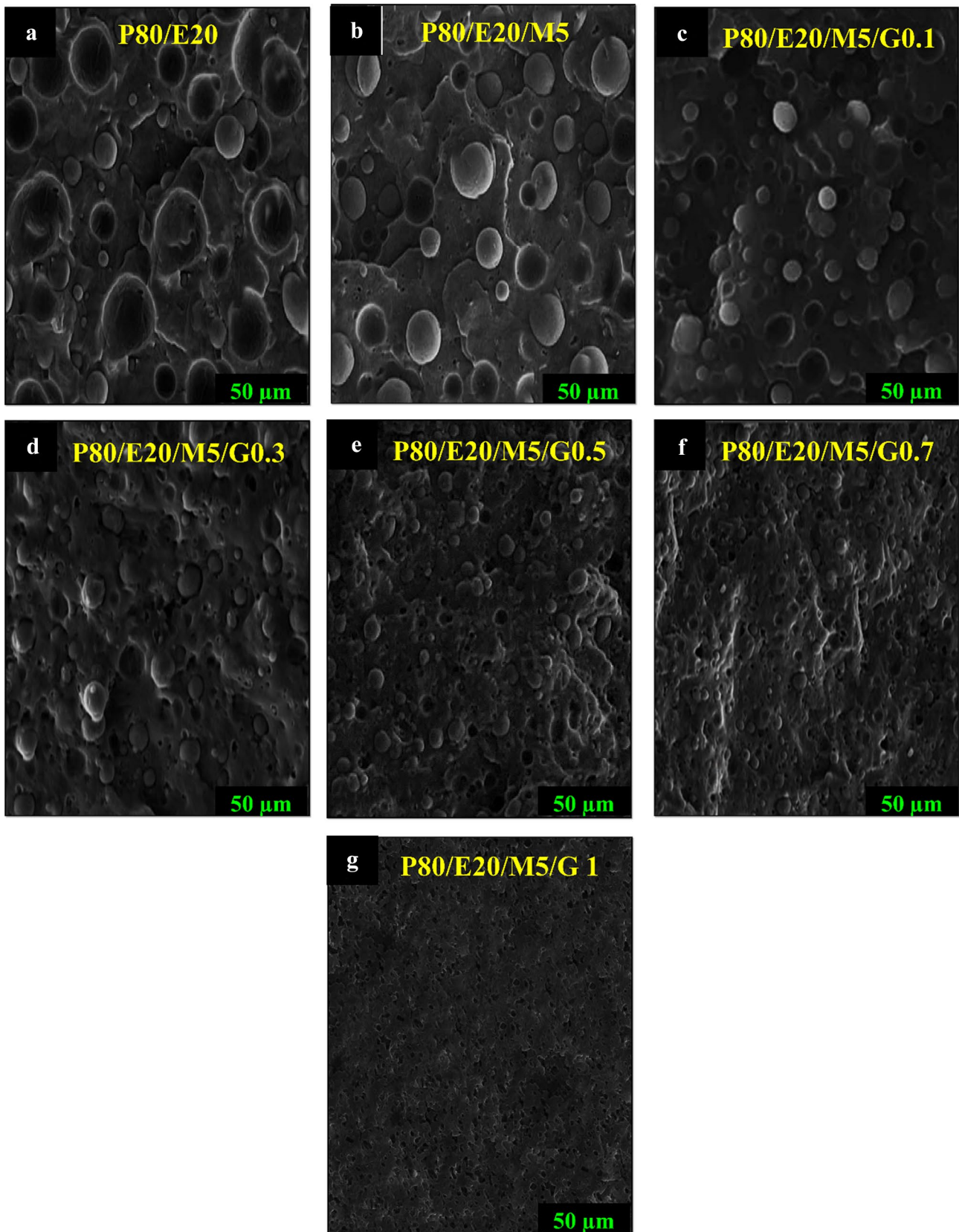
Fig. 3 The SEM micrographs of **a** P80/E20, **b** P80/E20/M5, **c** P80/E20/M5/G 0.1, **d** P80/E20/M5/G 0.3, **e** P80/E20/M5/G 0.5, **e** P80/E20/M5/G 0.7 and **e** P80/E20/M5/G 1 blends

graphene oxide in GO-PP/PP-g-MA/EPDM nanocomposites while at 1 phr graphene oxide, the properties do not raise and maybe the agglomeration of nanosheets [27]. These observations are following microscopic images. So that according to Fig. 4 increasing the graphene oxide concentration in the GO-PP/PP-g-MA/EPDM nanocomposites displays superb distribution.

The Christensen-Lo theory is used to predict the stiffness of nanocomposites containing shear and bulk moduli [28]:

$$K = K_p + \frac{\varphi(K_g - K_p)}{1 + (1 - \varphi)R_p(K_g - K_p) + X} \tag{5}$$

$$G = G_p + \frac{\varphi(G_g - G_p)}{1 + (1 - \varphi)Q_p(G_g - G_p) + Y} \tag{6}$$

where, the subscript g and p related to the GO and PP/PP-g-MA/EPDM, respectively. The φ is the effect of the interphase can be shown as follows [28]:

$$\varphi = \varphi_g + \varphi_i = (1 + \alpha)\varphi_g \tag{7}$$

where, φ_i and α is the volume fraction of interphase and interphase-dependent parameters, respectively. The two above parameters present the interfacial characteristics between GO and PP/PP-g-MA/EPDM. The α for filler reinforced polymers is introduced by [29]:

$$a = 3\left(\frac{r_i}{r_g}\right)\left(\frac{E_g - E_i}{E_g}\right) \tag{8}$$

In the above equations r_g, E_i and r_i are filler radius, interphase modulus and interphase radius, respectively. The main factor in the interphase modulus is the direction of nanoplatelets. The Y and X parameters are parameters attributed to the shear and bulk moduli of nanocomposite components, i.e. GO and PP/PP-g-MA/EPDM [30]:

$$X = \frac{a}{1 + R_g(K_p - K_g)} \tag{9}$$

$$Y = \frac{a}{1 + Q_g(G_p - G_g)} \tag{10}$$

In the above equations, Q_g and R_g are related to the GO nanosheets and G_p and R_p are related to the PP/PP-g-MA/EPDM blend are introduced by [30]:

$$R_Z = \frac{3}{3K_Z + 4G_Z} \tag{11}$$

$$G_Z = \frac{6(K_Z + 2G_Z)}{5G_Z(3K_Z + 4G_Z)} \tag{12}$$

The bulk and shear moduli of each GO and PP/PP-g-MA/EPDM with related to the elastic response of nanocomposite interphase calculated by [31]:

$$K_Z = \frac{E_Z}{3(1 - 2V_Z)} \tag{13}$$

$$G_Z = \frac{E_Z}{2(1 - V_Z)} \tag{14}$$

The elastic modulus of the nanocomposite interphase can be shown as follows [32]:

$$E_i(r) = E_p \times \frac{r_i}{r} + \left[\frac{r_i - r}{r_i - r_g}\right]^{\frac{\alpha}{2}} \times \left[E_g - E_p \times \frac{r_i}{r_g}\right] \tag{15}$$

The interphase young's modulus is determined as [33]:

$$E_i = \frac{1}{r_i - r_g} \times \int_{r_g}^{r_i} E_i(r)dr \tag{16}$$

The Kelly-Tyson model was used to predict the interphase thickness (r_i) from the experimental data [34]:

$$\sigma_n = \sigma_p[(B - 2.04)\left(1 + \frac{r_i}{r_g}\right)\varphi_g + 1 - \left(1 + \frac{r_i}{r_g}\right)^2 \varphi_g \tag{17}$$

In the above equation, σ_p, σ_n and φ_g are the tensile strength of PP/PP-g-MA/EPDM, the tensile strength of nanocomposite and GO level, respectively. B Parameter illustrated a quantitative determination for the filler–polymer interaction as [35]:

$$B = \frac{\ln(\frac{\sigma_n}{\sigma_p} \times \frac{1 + 2.5\varphi_g}{1 - \varphi_g})}{\varphi_g} \tag{18}$$

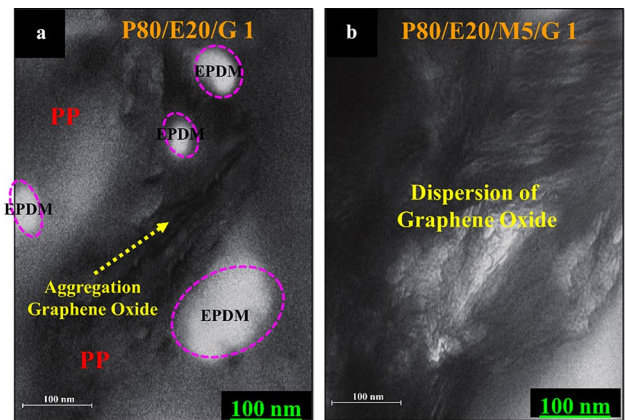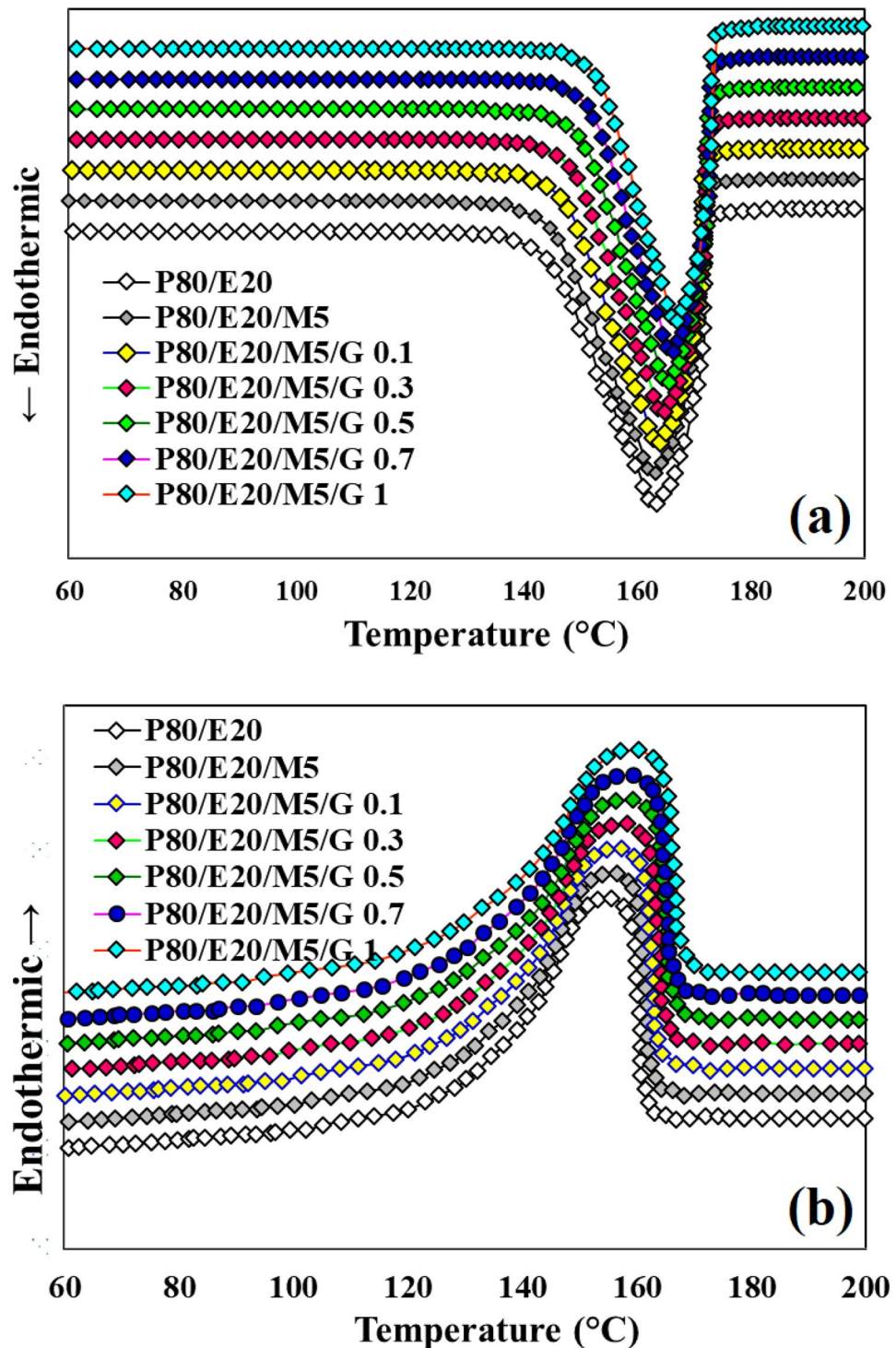The B parameter was set to an initial amount and will be determined by interphase modulus by iteration mechanism.

Fig. 4 The TEM of **a** P80/E20/G1 and **b** P80/E20/M5/G1

Fig. 5 Non-isothermal differential scanning calorimetry of cooling **a** and **b** heating curves and of the GO-PP/PP-g-MA/EPDM nanocomposites


At last, the predicted shear and bulk moduli may be calculated by the Christensen-Lo theory.

The elastic modulus predicted by GO-PP/PP-g-MA/EPDM nanocomposites is shown in Fig. 7. By applying of σ_n equation, the thickness of the interphase is determined by an experimental tension test. From Eqs. (8) and (15), the interaction parameter is first set to the initial amount and then determined by iteration mechanism. As can be seen, a proper accommodation presented between the predicted and the experimental results. There are some deviances from the experimental data, especially with raising graphene oxide content, because of the complex interactions in the structure, which cannot be fully determined by the proposed model.

Fig. 6 Thermal gravimetric analysis curves **a** and differential TG **b** of the GO-PP/PP-g-MA/EPDM nanocomposites
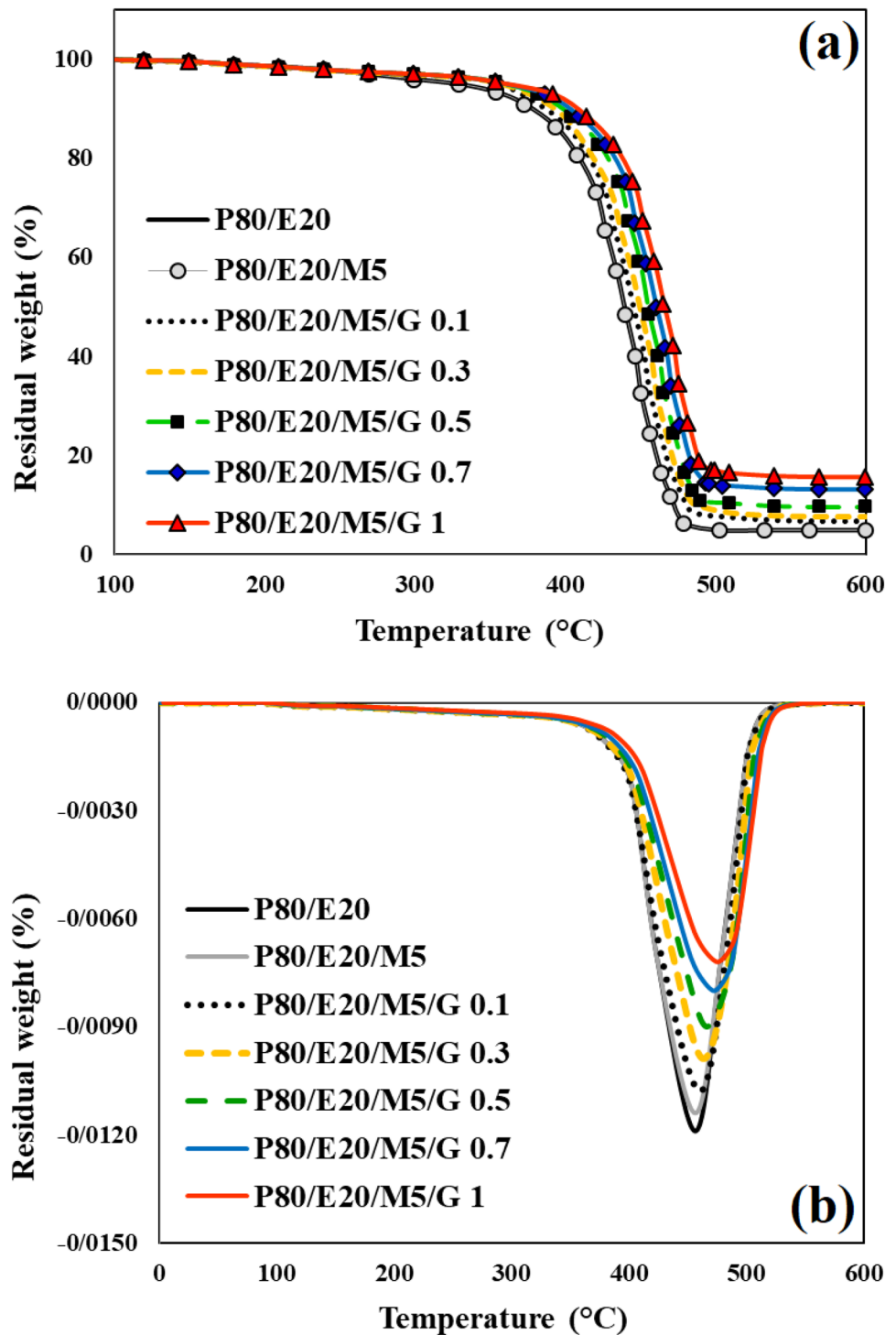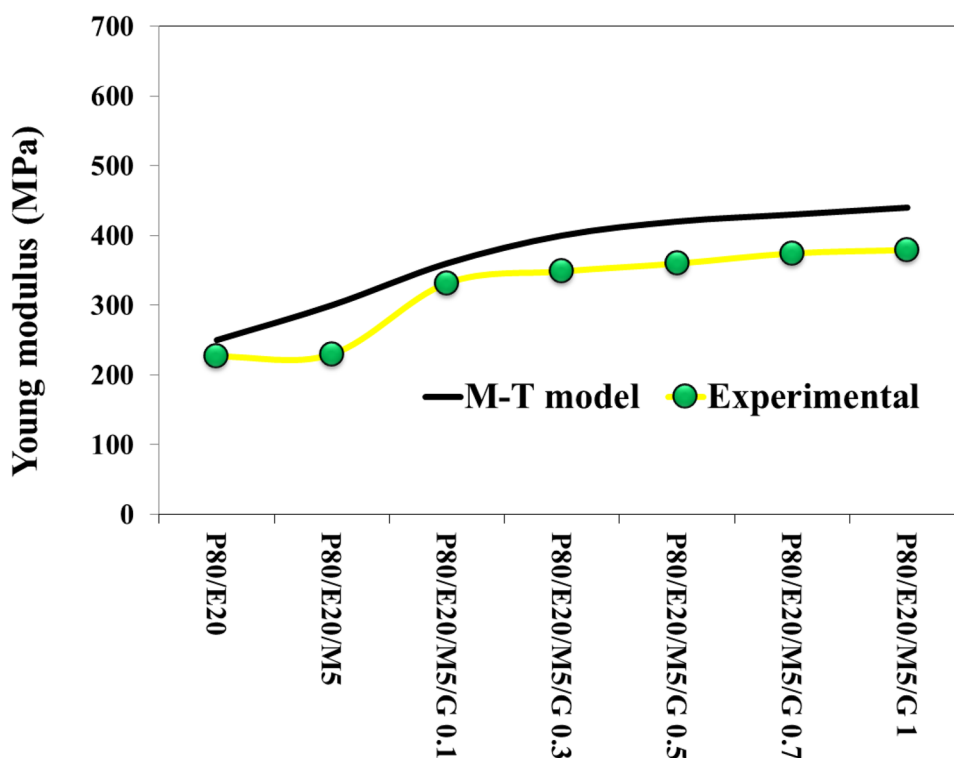

Loss factor and storage modulus characterization

Figure 8 shows the loss factor (tan δ) versus temperature for PP/EPDM-based compounds. In these curves, it seems that due to the incompatibility of two phase blends i.e. PP and EPDM, two distinct peaks with a certain height of these polymers are observed. But with the addition of PP-g-MA compatibilizer, a single peak with a certain height and glass transition temperature (Tg) is observed due to the compatibility between the two polymers in the presence of PP-g-MA between PP and EPDM phase blends. In addition, with the increase of graphene oxide in the PP/EPDM polymer matrix,

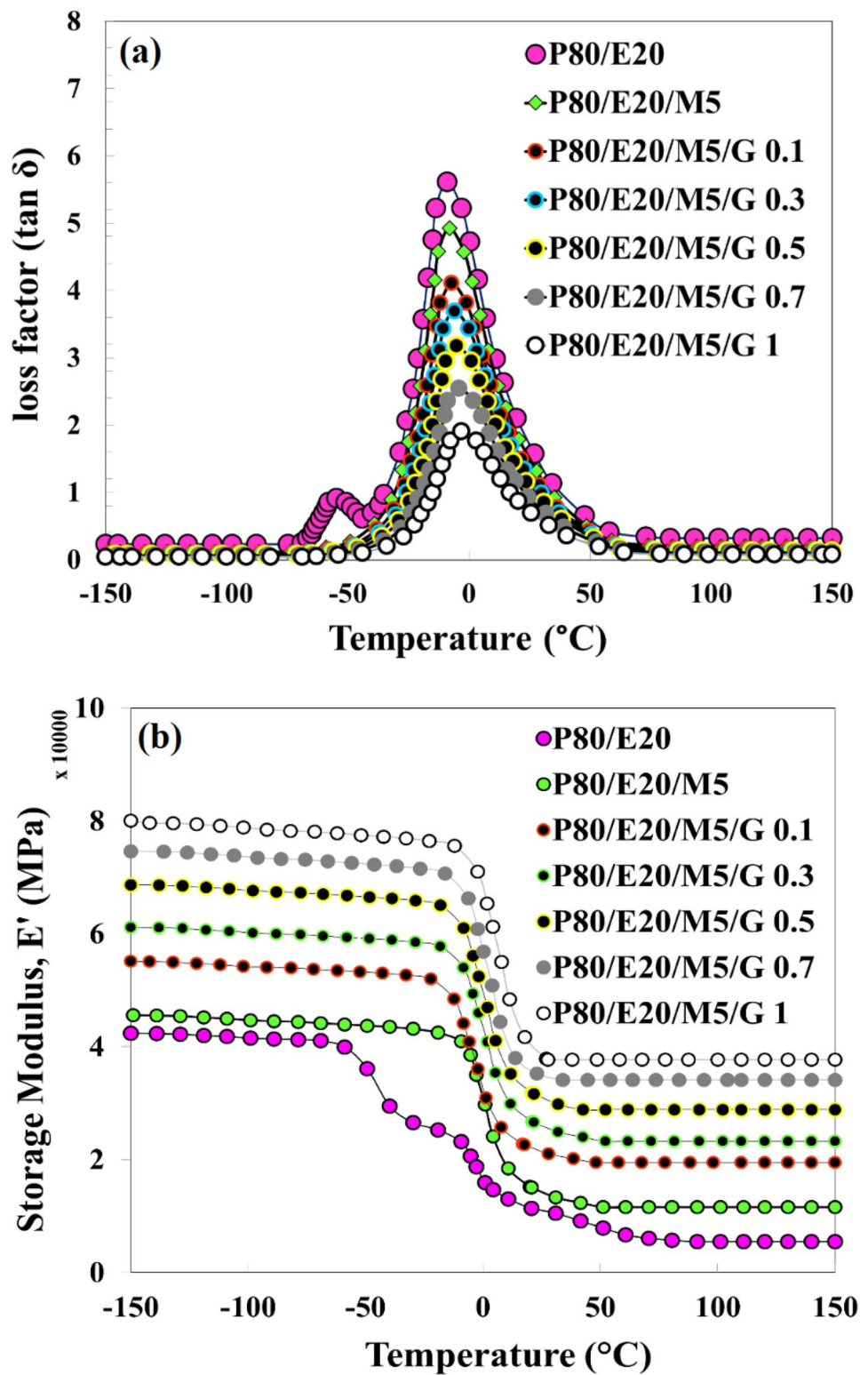**Fig. 7** Comparison of experimental data and proposed model for GO-PP/PP-g-MA/EPDM nanocomposites

Rheology measurements

The strain sweep results for PP/PP-g-MA/EPDM reinforced via the different amount of graphene oxide is shown in Fig. 9. As it can be seen, by increasing the frequency, the modulus increases, which is attributed to the incapacity of the matrix chains to pursue the applied shear [40]. On the other hand, the modulus of PP/EPDM enhances considerably via raising nanosheets at lower frequencies. Also, compatibilized P80/E20/M5/G1 nanocomposite illustrates 318% modulus growth at the frequency of 1 rad/s. However, the final steep of the modulus for nanocomposites is lower relationship with the proposed model than neat blends. This is attributed to the dispersion state of nanosheets arising from the powerful interactions between nanoparticles and polymeric chains. Another observation of Fig. 9 is that the shear thinning modus operandi of complex viscosity at lower shear rates of PP/EPDM. It is customary that the nanoparticles can enhance the shear thinning of neat polymers. This modus operandi shows that the nanoparticles are higher compatibilized to the polymer and illustrate stronger solid-like mode. Furthermore, raising the graphene oxide level in the polymer blends serves to the Newtonian behaviour of complex viscosity, leading to a primary beginning of shear thinning. Also, the viscosity and modulus show reverse behavior. This illustrates apparent yield stress, related to the establishment the networks of nanoparticles [41].

this trend seems to continue and only one peak of observation and peak height decreases. This is due to the limited mobility of the EPDM rubber phase chains and the PP plastic phase in the vicinity of the surface of graphene oxide nanosheets.

Figure 8 displays the storage modulus (E') graphs as a function of temperature for the nanocomposites based on the PP/EPDM blend. These curves confirm the loss factor (tan δ) data and show that the combination of PP/EPDM shows two peaks with two different Tg. But with the incorporation of the PP-g-MA compatibilizer, one peak and also one Tg are shown. Therefore, is created the compatibility between the two incompatible polymers i.e. PP and EPDM in the presence of the PP-g-MA compatibilizer. Also, with increasing the level of graphene oxide, the storage modulus is increased. The results of these two graphs are in good agreement with the results of TEM images (cf. to Fig. 4). According to Fig. 3. this may be due to the good interaction between nanocomposite ingredients and thus the formation of an intercalated and/or exfoliated structure in the GO-PP/PP-g-MA/EPDM matrix [36–39]. Table 6 reports the results for storage modulus and loss factor diagrams. As can be seen, with the addition of compatibilizer to the compounds, the number of glass transition temperatures is reduced from two to one, and with the incorporation and rasing of graphene oxide amount to the PP/EPDM blend matrix, the peak height is reduced, indicating improved interaction between the components in the presence of compatible and nanosheets.

Fig. 8 Loss factor (tan δ) **a** and storage modulus (E ') **b** of GO-PP/PP-g-MA/EPDM nano-composites


To obvious determination of the apparent yield stress of samples, the Herschel-Bulky model was applied:

$$\eta^* = \frac{G_0^*}{\omega} + K[\dot{\gamma}\omega]^{n-1} \qquad (19)$$

In the Eq. (19), G_0^*, K, $\dot{\gamma}$ and n are modulus at a frequency of 1 rad/s, power-law constant, shear rate and power-law index, respectively. On the other hand, the yield stress by having the initial modulus (G_0^*) and shear rate ($\dot{\gamma}$) can be calculated according to the Equation $\sigma_0 = G_0^* \dot{\gamma}$ [42]. The higher

Fig. 9 Storage modulus and complex viscosity of GO-PP/PP-g-MA/EPDM nanocomposites
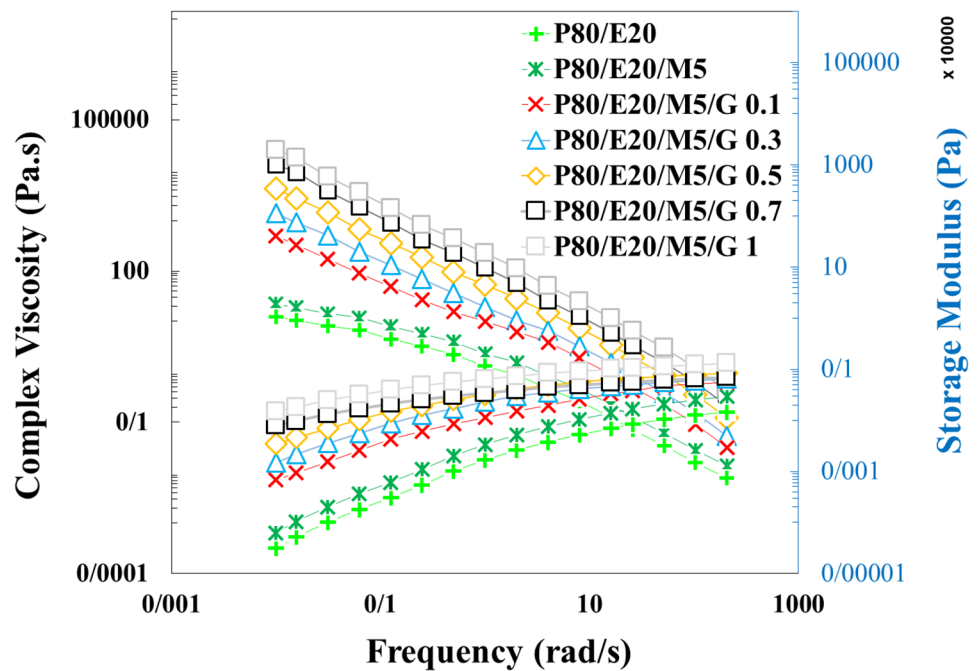
yield stress is attributed to the higher networks of nanoparticles and rubber-filler interactions. Table 7 tabulated the parameters of Herschel-Bulkley equation. It can be seen, by enhancement of graphene oxide amounts in PP/EPDM, the dispersion state of nanoparticles in the matrix raised with PP-g-MA compatibilizer, show better compatibility of polymer-filler in the GO-PP/PP-g-MA/EPDM nanocomposites.

Creep and Creep Recovery Analysis

In order to determination of dispersion mode of graphene oxide nanosheets via retardation data, creep and creep recovery tests were applied. The fixed value of shear stress was set at zero time up to 50 s and in parallel, shear stress as a function of time was calculated. Creep compliance was determined as [43]:

$$J(t) = \frac{\gamma^{(t)}}{\sigma_0} + J(t - t_0)t > t_0 \tag{20}$$

$$J_r = \frac{\gamma_r}{\sigma_0} = J_0 + \psi(t_r) = J_0 + \sum J_i(1 - e^{-t}/_{t_i}) \tag{21}$$

where, J_r is recoverable creep and γ_r is the recoverable strain. These two parameters are as a function of retardation time, t_r.

Figures 10a, b show the creep compliance and recoverable creep of PP/EPDM-based nanocomposites in the presence and absence of PP-g-MA compatibilizer. It is wholly obvious that in the presence of PP-g-MA compatibilizer and raising the nanoparticle amounts within PP/EPDM, the creep and recoverable creep illustrate lower amounts for neat PP/EPDM, which related to the rigid network of nanoparticles in the GO-PP/PP-g-MA/EPDM nanocomposites and consequence enhances the viscosity. Furthermore, as it can be seen, by increasing the GO nanoplatelets to the compounds, the recoverable creep (J_r) decreased. As can be seen in Eq. 21, J_r depends on the retardation time (t_r), and as retardation time decreases, the J_r decreases. Therefore, the nanocomposites containing a higher content of GO illustrate a lower amount of recoverable creep [44]. Also, the filler network in GO-PP/PP-g-MA/EPDM nanocomposites decreases the reversible strain because of the GO interactions. In contrast, a better exfoliation of nanoparticles within the polymeric matrix, the GO junctions are lower strained, hence the pressure on nanoparticles declines and thus the recoverable creep is diminished [45].

Fig. 10 creep compliance **a** and recoverable creep **b** of GO-PP/PP-g-MA/EPDM nanocomposites
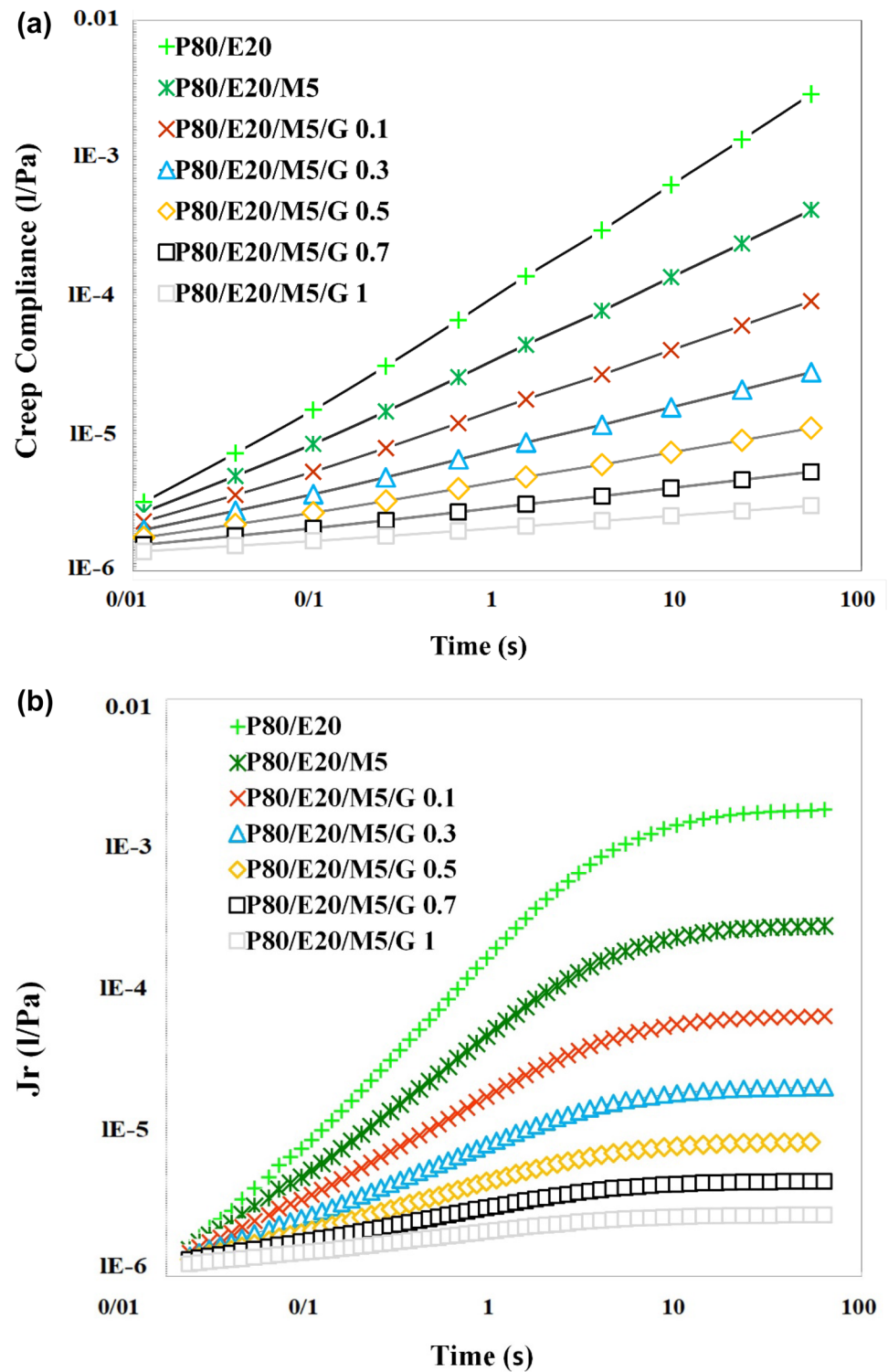
Conclusions

In this study, PP-g-MA compatibilizer was used to improve the compatibility of the immiscible PP/EPDM blend and graphene oxide nanosheets were used to improve the mechanical and thermal properties. TEM and SEM images and rheological, mechanical and thermal properties of pure PP/EPDM and GO-PP/PP-g-MA/EPDM nanocomposites were investigated. TEM images showed that the addition of PP-g-MA to the GO-PP/EPDM matrix resulted in well-dispersed of graphene oxide in the polymeric blend matrix. Rheometry results illustrated that the incorporation of graphene nanoparticles to the

neat blend, due to the reduction of chain mobility and their interaction with graphene nanoplatelets in the vicinity of the PP-g-MA compatibilizer, increased the modulus, especially in the lower frequency ranges. SEM micrographs of the nanocomposites showed a reduction in the dimensions of the EPDM dispersed phase droplets and their better distribution and/or dispersion in the PP matrix in the vicinity of the PP-g-MA compatibilizer with increasing graphene oxide. The results of mechanical characteristics showed that in samples with graphene oxide, the modulus increased and the elongation at break decreased. The increase in modulus is related to the higher hardness of graphene oxide-filled nanocomposites. Also, due to the high specific surface area of graphene nanosheets and the localization of them between the polymeric chains, the mobility and entanglement of the chains are reduced and slippage occurs, which reduces the flexibility of the chains and in turn the brittle behavior of the samples. The thermal stability of nanocomposites increased with increasing graphene oxide concentration. Compatibilized nanocomposites containing 1 phr of graphene nanoparticles showed higher crystallinity compared to the neat blend, which was attributed to the acceleration of nucleation by graphene nanosheets in the vicinity of the PP-g-MA compatibilizer.

Declarations

Conflict of interest The authors declare that they have no conflict of interest.

References

1. Pasquini N, Addeo A (2006) Polypropylene handbook. Choice Reviews Online 43:43–2825–43–2825. https://doi.org/10.5860/choice.43-2825

2. Hisham AM (2016) Polypropylene as a Promising Plastic: A Review. American Journal of Polymer Science 6:1–11

3. Paul DR (2012) POLYMER BLENDS, Volume 1. vol. 1. Elsevier

4. Xu C, Zheng Z, Wu W, Wang Z, Fu L (2019) Dynamically vulcanized PP/EPDM blends with balanced stiffness and toughness via in-situ compatibilization of MAA and excess ZnO nanoparticles: Preparation, structure and properties. Compos B Eng 160:147–157. https://doi.org/10.1016/j.compositesb.2018.10.014

5. Wu K, Wang X, Xu Y, Guo W (2020) Flame retardant efficiency of modified para-aramid fiber synergizing with ammonium polyphosphate on PP/EPDM. Polym Degrad Stab 172:109065. https://doi.org/10.1016/j.polymdegradstab.2019.109065

6. Niyaraki EN, Isvandzibaei MR, Niyaraki MN (n.d.) Experimental study of the impact and thermal properties of polypropylene/EPDM base nanocomposites reinforced with graphene nanosheets and nanoclay

7. Doufnoune R, Haddaoui N (2017) Effects of surface functionalized partially reduced graphene oxide and different compatibilizers on the properties and structure of PP/EPR nanocomposites. J Polym Res 24:138. https://doi.org/10.1007/s10965-017-1302-8

8. Chabot V, Higgins D, Yu A, Xiao X, Chen Z, Zhang J (2014) A review of graphene and graphene oxide sponge: Material synthesis and applications to energy and the environment. Energy Environ Sci 7:1564–1596. https://doi.org/10.1039/c3ee43385d

9. Razeghi M, Pircheraghi G (2018) TPU/graphene nanocomposites: Effect of graphene functionality on the morphology of separated hard domains in thermoplastic polyurethane. Polymer 148:169–180. https://doi.org/10.1016/j.polymer.2018.06.026

10. Haghnegahdar M, Naderi G, Ghoreishy MHR (2017) Fracture toughness and deformation mechanism of un-vulcanized and dynamically vulcanized polypropylene/ethylene propylene diene monomer/graphene nanocomposites. Compos Sci Technol 141:83–98. https://doi.org/10.1016/j.compscitech.2017.01.015

11. Díez-Pascual AM (2021) Effect of graphene oxide on the properties of poly(3-Hydroxybutyrate-co-3-Hydroxyhexanoate). Polymers 13:129. https://doi.org/10.3390/polym13142233

12. Azizli MJ, Barghamadi M, Rezaeeparto K, Mokhtary M, Parham S, Goodarzi V et al (2021) Enhancement of thermal, morphological, and mechanical properties of compatibilized based on PA6-enriched graphene oxide/EPDM-g-MA/CR: Graphene oxide and EPDM-g-MA compatibilizer role. J Appl Polym Sci 138:49901. https://doi.org/10.1002/app.49901

13. Pan Q, Shim E, Pourdeyhimi B, Gao W (2017) Highly Conductive Polypropylene-Graphene Nonwoven Composite via Interface Engineering. Langmuir 33:7452–7458. https://doi.org/10.1021/acs.langmuir.7b01508

14. Yao J, Liu S, Huang Y, Ren S, Lv Y, Kong M et al (2020) Acyl-chloride functionalized graphene oxide chemically grafted with hindered phenol and its application in anti-degradation of polypropylene. Progress in Natural Science: Materials International 30:328–336. https://doi.org/10.1016/j.pnsc.2020.05.010

15. Tripathi S, Bhattacharya A, Singh R, Tabor RF (2017) Rheological behavior of high internal phase water-in-oil emulsions: Effects of droplet size, phase mass fractions, salt concentration and aging. Chem Eng Sci 174:290–301. https://doi.org/10.1016/j.ces.2017.09.016

16. Esmizadeh E, Sadeghi T, Vahidifar A, Naderi G, Ghoreishy MHR, Paran SMR (2019) Nano Graphene-Reinforced Bio-nanocomposites Based on NR/PLA: The Morphological, Thermal and Rheological Perspective. J Polym Environ 27:1529–1541. https://doi.org/10.1007/s10924-019-01450-x

17. Bazli L, Barghamadi M, Shafiee S, Karrabi M, Ghoreishy MHR (2021) Investigation of rheological, mechanical, and thermal properties of nanocomposites based on nitrile rubber-phenolic resin reinforced with nanographene. J Appl Polym Sci 138:50906. https://doi.org/10.1002/app.50906

18. Scaffaro R, Maio A, Gulino EF, Morreale M, La MFP (2020) The effects of nanoclay on the mechanical properties, carvacrol release and degradation of a pla/pbat blend. Materials 13:983. https://doi.org/10.3390/ma13040983

19. McKeen LW (2017) Film properties of plastics and elastomers. William Andrew

20. Azizl MJ, Barghamadi M, Rezaeeparto K, Mokhtary M, Parham S (2021) Graphene oxide and graphene hybrid nanocomposites based on compatibilized PP/PTW/EVA: effect of nanofiller and compatibilizer on the modeling of viscoplastic behavior. J Polym Res 28:1–21. https://doi.org/10.1007/s10965-021-02647-2

21. Patra PK, Jaisingh A, Goel V, Kapur GS, Nebhani L (2021) Crystallization kinetics of compatibilized blends of polypropylene and polyethylenimine. J Thermal Anal and Cal 1–11. https://doi.org/10.1007/s10973-021-10970-5

22. Li X, Bandyopadhyay P, Nguyen TT, Park O kyung, Lee JH (2018) Fabrication of functionalized graphene oxide/maleic anhydride grafted polypropylene composite film with excellent gas barrier and anticorrosion properties. J Memb Sci 547:80–92. https://doi.org/10.1016/j.memsci.2017.10.031

23. Hasanzadeh Kermani H, Mottaghitalab V, Mokhtary M, Alizadeh DA (2020) Morphological, rheological, and mechanical properties of ethylene propylene diene monomer/carboxylated styrene-butadiene rubber/multiwall carbon nanotube nanocomposites. Int J Polym Anal Charact 25:479–498. https://doi.org/10.1080/1023666X.2020.1807681

24. Xue C, Gao H, Hu Y, Hu G (2019) Hyperelastic characteristics of graphene natural rubber composites and reinforcement and toughening mechanisms at multi-scale. Compos Struct 228:111365. https://doi.org/10.1016/j.compstruct.2019.111365

25. Barghamadi M, Karrabi M, Ghoreishy MHR, Mohammadian-Gezaz S (2019) Effects of two types of nanoparticles on the cure, rheological, and mechanical properties of rubber nanocomposites based on the NBR/PVC blends. J Appl Polym Sci 136. https://doi.org/10.1002/app.47550

26. Azizli MJ, Barghamadi M, Rezaeeparto K, Mokhtary M, Parham S (2020) Compatibility, mechanical and rheological properties of hybrid rubber NR/EPDM-g-MA/EPDM/graphene oxide nanocomposites: Theoretical and experimental analyses. Composites Communications 22:100442. https://doi.org/10.1016/j.coco.2020.100442

27. Yang H, Cai F, Luo Y, Ye X, Zhang C, Wu S (2020) The interphase and thermal conductivity of graphene oxide/butadiene-styrene-vinyl pyridine rubber composites: A combined molecular simulation and experimental study. Compos Sci Technol 188:107971. https://doi.org/10.1016/j.compscitech.2019.107971

28. Zare Y (2015) Assumption of interphase properties in classical Christensen–Lo model for Young's modulus of polymer nanocomposites reinforced with spherical nanoparticles. RSC Adv 5:95532–95538

29. Raos G (2003) Application of the Christensen-Lo Model to the Reinforcement of Elastomers by Fractal Fillers. Macromol Theory Simul 12:17–23

30. Zare Y (2016) A model for tensile strength of polymer/clay nanocomposites assuming complete and incomplete interfacial adhesion between the polymer matrix and nanoparticles by the average normal stress in clay platelets. RSC Adv 6:57969–57976

31. Budiansky B (1965) On the elastic moduli of some heterogeneous materials. J Mech Phys Solids 13:223–227

32. Chu YC, Rokhlin SI (1995) Determination of fiber-matrix interphase moduli from experimental moduli of composites with multilayered fibers. Mech Mater 21:191–215

33. Shen L, Li J (2005) Homogenization of a fibre/sphere with an inhomogeneous interphase for the effective elastic moduli of composites. Proceedings of the Royal Society A: Mathematical, Physical and Engineering Sciences 461:1475–1504

34. Zare Y (2015) Effects of interphase on tensile strength of polymer/CNT nanocomposites by Kelly-Tyson theory. Mech Mater 85:1–6

35. Jiang B, Weng GJ (2004) A generalized self-consistent polycrystal model for the yield strength of nanocrystalline materials. J Mech Phys Solids 52:1125–1149

36. Barghamadi M, Ghoreishy MHR, Karrabi M, Mohammadian-Gezaz S (2021) Modeling of nonlinear hyper-viscoelastic and stress softening behaviors of acrylonitrile butadiene rubber/polyvinyl chloride nanocomposites reinforced by nanoclay and graphene. Polym Compos 42:583–596. https://doi.org/10.1002/pc.25849

37. Biranje PM, Prakash J, Srivastava AP, Biswas S, Patwardhan AW, Joshi JB et al (2021) In situ tuning of graphene oxide morphology by electrochemical exfoliation. J Mater Sci 56:19383–19402. https://doi.org/10.1007/s10853-021-06535-4

38. Barghamadi M, Ghoreishy MHR, Karrabi M, Mohammadian-Gezaz S (2020) Investigation on the kinetics of cure reaction of acrylonitrile–butadiene rubber (NBR)/polyvinyl chloride (PVC)/graphene nanocomposite using various models. J Appl Polym Sci 137. https://doi.org/10.1002/app.48632

39. Xia Z, Maccaferri G, Zanardi C, Christian M, Ortolani L, Morandi V et al (2019) Dispersion Stability and Surface Morphology Study of Electrochemically Exfoliated Bilayer Graphene Oxide. J Phys Chem C 123:15122–15130. https://doi.org/10.1021/acs.jpcc.9b03395

40. Sharma RP, Green PF (2017) Component Dynamics in Polymer/Polymer Blends: Role of Spatial Compositional Heterogeneity. Macromolecules 50:6617–6630. https://doi.org/10.1021/acs.macromol.7b00092

41. Sangroniz L, Santamaría A, Müller AJ (2019) Rheology of polymer blend nanocomposites. Rheol Polym Blends and Nanocompos: Theory, Modelling and App Elsevier 123–60. https://doi.org/10.1016/B978-0-12-816957-5.00007-0

42. Manzoor MF, Ahmad N, Aadil RM, Rahaman A, Ahmed Z, Rehman A et al (2019) Impact of pulsed electric field on rheological, structural, and physicochemical properties of almond milk. J Food Process Eng 42:e13299. https://doi.org/10.1111/jfpe.13299

43. Wang Z-N, Shen S-L, Zhou A, Lyu H-M (2021) Investigation of Time-Dependent Characteristics of EPDM Rubber Gasket Used for Shield Tunnels. J Mater Civ Eng 33:04021251. https://doi.org/10.1061/(asce)mt.1943-5533.0003844

44. Sakib N, Koh YP, Huang Y, Mongcopa KIS, Le AN, Benicewicz BC et al (2020) Thermal and Rheological Analysis of Polystyrene-Grafted Silica Nanocomposites. ACS Appl Mater Interfaces 53:2123–2135. https://doi.org/10.1021/acs.macromol.9b02127

45. Azarhoosh A, Koohmishi M (2020) Investigation of the rutting potential of asphalt binder and mixture modified by styrene-ethylene/propylene-styrene nanocomposite. Constr Build Mater 255:119363. https://doi.org/10.1016/j.conbuildmat.2020.119363